General fabrication of ordered nanocone arrays by one-step selective plasma etching

2014 Nanotechnology 25 115301

(http://iopscience.iop.org/0957-4484/25/11/115301)

IOP Publishing Nanotechnology
Nanotechnology **25** (2014) 115301 (10pp) doi:10.1088/0957-4484/25/11/115301

General fabrication of ordered nanocone arrays by one-step selective plasma etching

Qiang Wang[1], Zhaoshuo Tian[1], Yunlong Li[2], Shibing Tian[2], Yunming Li[2], Shoutian Ren[1], Changzhi Gu[2] and Junjie Li[2]

[1] Department of Optics and Electronics Science, College of Science, Harbin Institute of Technology at Wei Hai, Wei Hai 264209, People's Republic of China
[2] Beijing National Laboratory for Condensed Matter Physics, Institute of Physics, Chinese Academy of Sciences, Beijing 100190, People's Republic of China

E-mail: wq750505@hotmail.com and jjli@iphy.ac.cn

Received 4 November 2013, revised 9 December 2013
Accepted for publication 3 January 2014
Published 20 February 2014

Abstract

One-step selective direct current (DC) plasma etching technology is employed to fabricate large-area well-aligned nanocone arrays on various functional materials including semiconductor, insulator and metal. The cones have nanoscale apexes (~2 nm) with high aspect ratios, which were achieved by a selective plasma etching process using only CH_4 and H_2 in a bias-assisted hot filament chemical vapor deposition (HFCVD) system without any masked process. The CH_3^+ ions play a major role to etch the roughened surface into a conical structure under the auxiliary of H^+ ions. Randomly formed nano-carbon may act as an original mask on the smooth surface to initiate the following selective ions sputtering. Physical impinging of energetic ions onto the concave regions is predominant in comparison with the etching of convex parts on the surface, which is identified as the key mechanism for the formation of conical nanostructures. This one-step maskless plasma etching technology enables the universal formation of uniform nanocone structures on versatile substrates for many promising applications.

Keywords: general cones formation, one-step selective plasma etching, methylic $CH_3{}^+$ ions, nano-masking

(Some figures may appear in colour only in the online journal)

1. Introduction

Controlled preparations of large-scale ordered surface micro/nano-structures are essential research issues in nanoscience and nanotechnology, which can be performed by following either a bottom-up growth method or a top-down etching scheme. The latter is usually realized in the context of plasma-assisted nanofabrication, which can be managed through the adjustment of the major elementary reactions in the plasma by varying the discharge control parameters [1]. Therefore, low-temperature and low-energy plasma generated by low-pressure direct current (DC) gas discharge is widely recognized as a versatile and efficient tool for large-scale fabrication of ordered surface structures, such as pillars, wires, cones, tips, etc. As-fabricated surface structures with ordered array can be used in many fields such as vacuum electron emitters, anti-reflection layers, super-hydrophobic layers, optoelectronic and photonic devices, nonvolatile data storage elements, nanoelectronic integrated circuits, nonvolatile data storage elements, nanoelectronic integrated circuits, biosensors, Raman enhancement substrates, as well as protein and cell immobilization arrays [2–6].

An ordered conical structure (or nano-tips array) has been especially relevant in recent years due to the promising applications in many fields [7–14]. In order to fabricate nanocone arrays by using the subtractive method, several methods have been tried such as the Spindt method, the plasma etching method combined with masking technology, and laser evaporation of substrates, etc [15–18]. But the above-mentioned methods can only be applied to limited materials and areas,

and involve high experimental cost and rather complicated technologies, such as the lithography, patterned masking and the lift-off. In recent years, dry plasma etching technology without pre-masking for one-step formation of cone arrays on different substrates had been studied intensively [19–21]. This method shows particular potentials in the formation of an ordered large-area nanocones array, and had been testified to be an economical and efficient technique.

Black silicon is a typical material formed by this one-step plasma etching method to form silicon cone or 'grass' on silicon wafer [22]. Black silicon is mostly formed without intentional masking, but instantaneous masking materials such as SiO_2 nanoparticles, water chemisorbing products as SiOH or SiH species, chamber contamination particles, and even plasma generated metal nanoparticles from filaments were sometime proposed to explain the observed formation of silicon cones or tips [22, 23]. As far as we know, the methods that were used to form black silicon involve laser ablation, reactive ions etching, etc, which encounter such shortcomings as severe surface destruction and non-universality. In addition, the above one-step etching methods are only suitable for the fabrication of a silicon cones structure rather than other materials. To note another example [24, 19], for general cone formation without intentional masking, it had been proposed that as-formed nano-particles, such as oxides, SiC, etc, dwelling on the flat substrate surface will act as a nanoscaled mask, which would protect the underlying parts from etching, and therefore induce the development of a conical structure. Yet the above mechanisms are not consistent with the experimental results that no masking nano-particles had been found dwelling on the top of as-formed cones, basing on the detailed TEM examination [20, 25]. Other results have been reported to show the decisive role of self-organized selective ion bombardment for a roughened surface [26, 27], yet few systematic studies of the relation between the cone morphology and experimental parameters have been presented so far. In order to develop the production techniques with industrial interest, a universal one-step plasma etching for versatile substrates should be developed as a new technical strategy, and a thorough understanding of the mechanisms governing the formation of ordered conical nanostructure without pre-masking is very necessary.

In this work, we report a selective ion-sputtering process for the universal formation of large-area conical nanostructure arrays on versatile substrates, such as metals, semiconductors and insulators, using a hot filament chemical vapor deposition (HFCVD) system to generate DC plasma. The uniform nanocone arrays can be formed on originally either a smooth or roughened surface, and the cones' morphologies can be modified by originally patterned surface nanostructures. The self-organized selective sputtering process of as-formed hillock bottoms on a roughened surface by low-energy ions plays a key role for the formation and development of surface cones. Commonly used CH_4 and H_2 are selected as plasma gas, in which methylic ions (CH_3^+) dominantly contribute to the cone formation, which introduces many unique technical advantages such as cheapness, universality, non-toxicity and simplicity.

2. Experimental details

Nanocones can be formed on different substrates in a widely opened parameters window of DC plasma, and the structure parameters (height, cone angle, density, etc) of as-formed cones can be intentionally controlled by changing plasma parameters [20, 28]. In our experiments, all kind cone arrays were fabricated by using a HFCVD system equipped with a negatively biased DC voltage system. A Ta wire with a diameter of 0.9 mm is used as a filament, and is heated to about 2100 °C. The inter-electrode distance is modulated to 2100 °C. The inter-electrode distance is modulated to about 8 mm between the cathode Ta filament and the cathode substrate, which results in the substrate temperature of about 800 °C. A negatively biased voltage of 300 V is applied on the substrate for generation of glow discharge using a DC constant voltage source. For investigating the relations between the experimental parameters and as-formed cone morphologies, serial experimental parameters were designed. Because many parameters are inter-involved and coupled with each other, the optimization of experiments is not always easy. At 800 °C, the precursor gas CH_4/H_2 with different volume ratios of 1.5/98 and 0/100, is introduced into the chamber, the growth pressure is changed from 15 to 30 Torr, and the growth duration is ranged from 1 to 10 h. In our experiments, several kinds of substrates are put onto the cathode sample holder to be etched, including silicon, diamond, SiC, ZnO, AlN, and metal Cu. As should be noted, for rather insulating materials (SiC, ZnO and diamond slice) it is beneficial to cut them into small sizes to facilitate plasma generation on their surface. Yet for diamond and AlN film grown on n-type silicon (5–10 Ω cm), plasma generation is much easier due to the availability of defect-induced conducting sites.

After the formation of cone arrays, the samples are immediately characterized. The morphologies of as-formed diamond cone arrays are studied using the scanning electrons microscopy (SEM) by tilting the sample holder with an angle of 52°. Chemical bonding of an as-formed diamond cone is investigated by using a JY-T64000 Micro-Raman spectroscopy system with Ar^+ laser excitation (514.5 nm). The cone microstructure is studied by using high-resolution transmission electrons microscopy (HRTEM).

3. Results and discussion

3.1. Morphologies of conical structures on different substrate materials

Based on the universal one-step selective plasma etching, different conical structures are fabricated on various substrate materials, which include Si wafer, diamond films, SiC wafer, ZnO slice, AlN film and Cu foil. The morphologies of as-fabricated cones are described in this section.

Silicon cones are formed on a n-type (100) crystalline silicon wafer 4 in. in size. Figures 1(a) and (b) show the SEM images of Si cones on the wafer and TEM images of a single cone, respectively. As can be seen from the optical image of the whole silicon wafer in figure 1(a), the center region is black

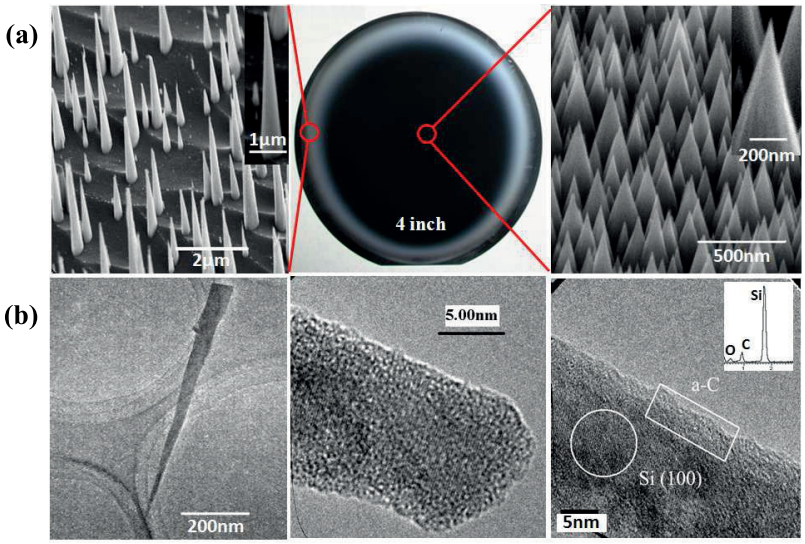

Figure 1. Silicon cones on crystalline silicon wafer. (a) The optical image of Si cone on the 4 in. wafer (middle), SEM images of Si cones on the wafer edge region (left) and wafer center region (right), and two insets SEM images showing the selected cones with higher resolution; (b) TEM images of a single Si cone (left), the top of Si cone (middle) and the middle part of the Si cone (right) with a inset of the EDX result.

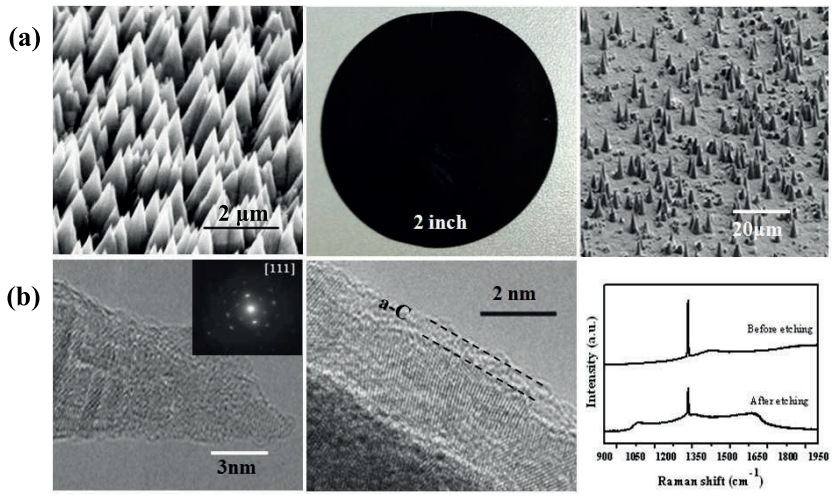

Figure 2. Diamond cones on crystalline silicon wafer. (a) The optical image of diamond cone on the 2 in. wafer (middle), SEM images of diamond cones on the wafer edge region (left) and wafer center region (right); (b) TEM images of a single diamond cone for the tip region (left), the sidewall (middle) and the Raman spectra of diamond film before and after plasma etching (right).

and the edge is gray-white. The optical reflective properties are related with the cone population density and cone size of different regions. Once the feature size of as-formed cones becomes smaller than the wavelength of visible light, the surface appears black due to its anti-reflective property. In the wafer edge region, the cones show an average height of $\sim$4 μm and cone distribution density of $\sim$0.15 cones μm^{-2}. In the center region, the cones show an average height of less than $\sim$1.5 μm, and the cone population density is about 4 cones μm^{-2}. By comparison, we can see the cones in the edge regions are greatly sharpened, except for the larger cone size and lower population density, which indicates the ions' distribution in the whole plasma sheath around the silicon wafer is not uniform, and the electric field in the edge region is greatly strengthened due to the geometry-induced edge-effect. However, a uniform and stable electric field distribution can still be realized on the majority of the wafer, and hence a well-distributed Si cones array can be formed. As can be seen in figure 1(b), the TEM images show that the tip radius of a silicon cone is about 5 nm, and amorphous carbon (a-C) coating on the cone surface is detected, which is certified by an inset in the EDX results. In addition, any masking particles are not found on the cone tip from the above TEM characterization.

Similar experimental results are also observed on as-etched diamond film with the thickness of about 10 μm grown on silicon wafer. Diamond cones with different morphologies are formed on different regions of the substrate. Figure 2(a) shows the optical image (middle) of diamond cones on 2 in. wafer, and SEM images of cones on the wafer center (left) and edge regions (right) are also shown respectively, indicating that uniform high-density cone arrays are formed in the center region while there are some discrete and larger cones

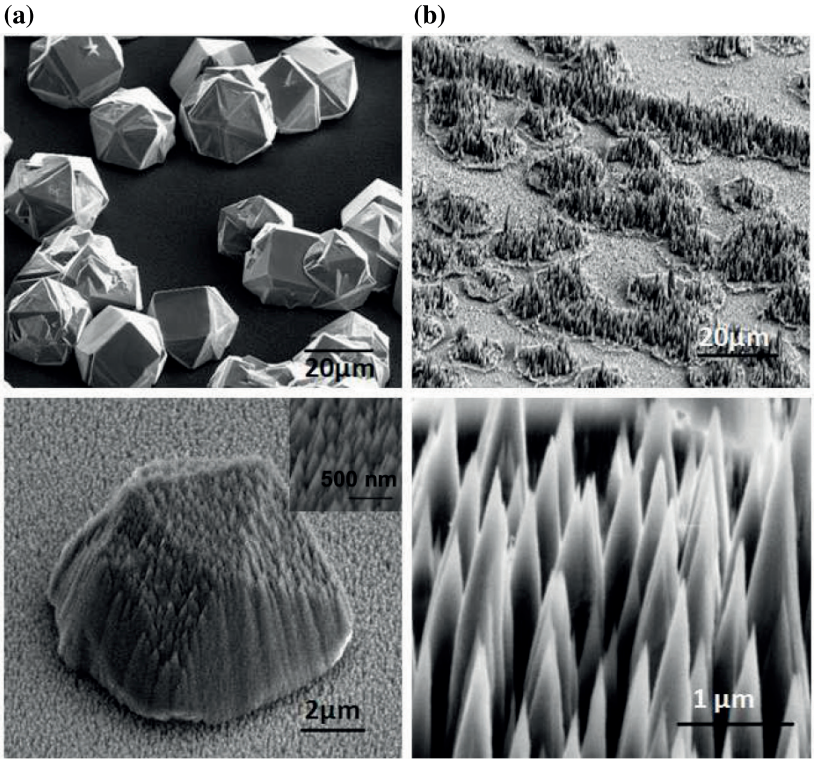

Figure 3. Diamond nanocones formed by etching discretely populated diamond particles grown on crystalline silicon wafer by pure hydrogen plasma (a) and CH_4/H_2 plasma (b), respectively.

in the edge region. Figure 2(b) shows the microstructures of diamond cone using a TEM study (left and middle), and the changes of Raman scattering signals for the sample before and after etching, are also shown (right). As we can see, the diamond cone has a tip radius of 1–2 nm, showing crystalline structures with [111] orientation. Surface coating of a-C is also detected by TEM study, which is further verified by Raman spectra measurement. The characteristic peak of diamond at 1332 cm^{-1} is weakened after the etching process, and a new peak appearing at about 1610 cm^{-1}, assigning to sp^2-rich a-C, is detected. The peak at about 1050 cm^{-1} is assigned to secondary order scattering of optical phonons in silicon, revealing silicon substrate by the ions etching.

In order to determine the etching process (not the growth scheme) for cones formation, isolated diamond particles grown on silicon surface by the HFCVD method are also employed. The upper image in figure 3(a) shows the SEM result of isolated diamond particles grown on silicon before etching. The lower image in figure 3(a) shows the SEM result of an isolated diamond particle after etching in pure H_2 plasma, being inset with the high-resolution image of the as-etched nanocones on the diamond particle. The as-etched diamond film still remains the original morphologies with only the presence of grassy surface nano-structures. If methane is added into the plasma, the etching rate can be greatly enhanced. The upper image in figure 3(b) shows the SEM image of the sample after CH_4/H_2 plasma etching. As we can see, the protruding diamond particles are apparently etched into sparse and large cones on the substrate; while the underlying silicon surface remains almost intact (only grassy nano-tips can be detected). As should be noted here, it is mainly due to the much different etching rate of diamond particles and silicon wafer in the carbon-containing plasma, and it should not be confused with the following mechanism discussion of different sputtering rates of the convex and concave regions. The lower image in figure 3(b) shows the SEM result of an isolated diamond particle etched by CH_4/H_2 plasma, showing diamond cones with height larger than 5 μm. Comparing the different results shown in figure 3(a) and (b), it clearly shows that the addition of methane plays a key role for the formation of large cones, which is in good consistency with our previous published result that the methane ions CH_3^+ exhibit a much greater selective etching rate than H^+ ions [20].

At some optimized experimental conditions, diamond cones on CVD free-standing thick diamond film can be formed with height above 30 μm. The rather large cone size results from the much larger size of diamond particles. We should note that the thick diamond films are highly resistive, but large cones can still be formed in the edge regions of the substrate. This kind of large cone may be applied as an ultra-hard probe in many fields, only if they can be well peeled, transferred and reloaded.

At optimized experimental conditions, conical structures can also be formed on different kinds of substrates like SiC wafer, Cu foil, AlN film on silicon and ZnO ceramic slice. All samples are formed at 800 °C using a mixed gas of CH_4/H_2 with a volume ratio of 1.5/98. Figure 4(a) show the cones array formed on SiC wafer, and the needle-like cones show an average height of about 3 μm. The etching gas pressure is kept at 15 Torr and etching duration is about 4 h. Figure 4(b)

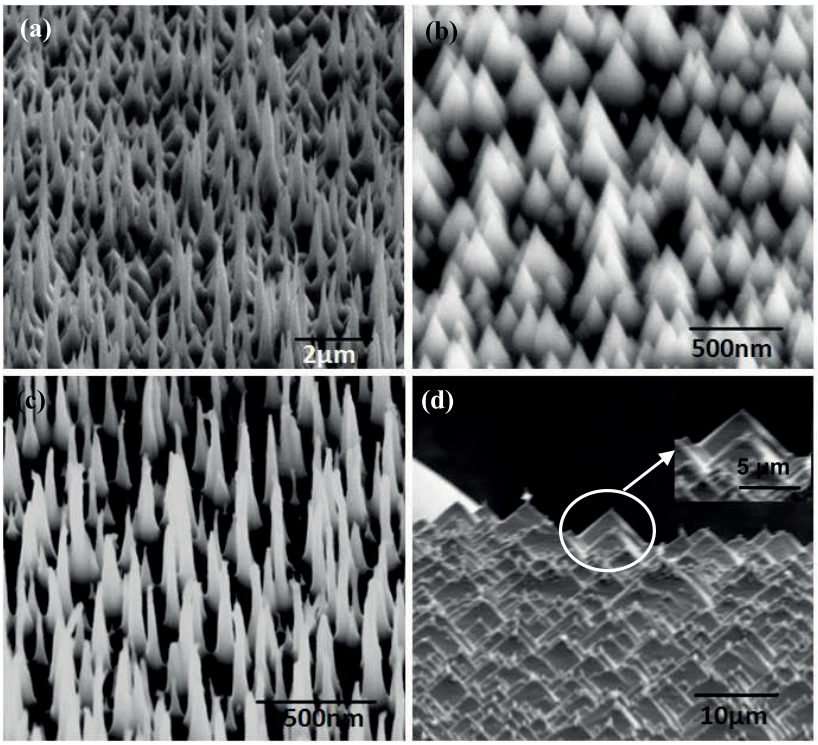

Figure 4. Nanocones formed by etching of (a) SiC wafer, (b) Cu foil, (c) AlN (d) ZnO film substrate all at 800 °C and mixed gas of CH_4/H_2 (with volume ratio of 1.5/98).

shows the nano-tip arrays with size of 200 nm formed on copper foil substrate. The etching gas pressure is kept at 10 Torr and etching duration is about 2 h. Figure 4(c) shows the cones array formed by etching of AlN film grown on silicon wafer. We can see that the AlN film is etched into a densely populated nano-tips array with high aspect ratio. The etching gas pressure is kept at 20 Torr and etching duration is about 5 h. Plasma etching of ZnO slice is also performed, and conical surface structures are also formed on the original smooth surface, having a low height and large cone angle (even larger than 90°), as shown in figure 4(d). The etching gas pressure is kept at 25 Torr and etching duration is about 5 h for formation of ZnO cone. The cones show rather different morphologies by etching of different materials at somehow similar experimental parameters, which indicates the atom mass, electrical conductivity, melting point, and many other physical properties of materials may effectively modify the as-etched cone morphologies. In any case, the cone formation is a universal phenomenon in our experiments, and thus the underlying mechanism of the cone formation is very important to understand the whole etching process.

3.2. Cones formation modeling

To theoretically establish the cones formation model for a universal one-step selective plasma etching process, various factors should be considered, such as the evidence of selective etching, the control of cone angle, the role of CH_3^+ ions, the effect of original substrate nanostructures and the occurrence of instantaneous masking, etc. Patterned silicon wafers using reactive ions etching (RIE) are used as the substrates to implement one-step selective plasma etching, as shown in figure 5. As we can see, nano-tips are always formed preferentially in the lower parts of the patterned silicon wafer. Above phenomena provide strong evidence that the cones' formation follows a geometrically selective mechanism: upon energetic ions bombardment, the regions in the lower position show a higher etching rate to develop larger cones.

Cone angle is one of the typical characteristics of cone structure, which is dependent on the control of ion etching parameters. Here, an interesting statistical distribution of silicon cone angle for two samples etched in the mixed ambience of CH_4 and H_2 with a volume ratio of CH_4:$H_2 = 1.5$:98.5 is shown in figure 6. As can be seen, the averaged cone angle is about 27° (with statistical error of about 6.5°) at a gas pressure of 5 Torr, and it is about 52° (with a statistical error of about 6°) at a gas pressure of 30 Torr. Cone formation is a natural occurrence by ion sputtering if there are contaminations or precipitate particles on the substrate surface. When the shielding particles are eroded away, the surface is covered with cones or steps. It had been pointed out theoretically that the dependence of the sputtering yield S on the angle of incidence θ could be responsible for the observed cones on the bombarded surface. This classical theory is based on the motion of two intersecting planes during ion erosion, and the planes inclined at an angle θ_p were produced by the etching at an angle where the erosion had the maximum yield. The angular dependence of sputtering yield S is expressed as the following [29]:

$$S(\theta) = (\pi^2/4)sa^2nE_aR\sec\theta \quad (1)$$

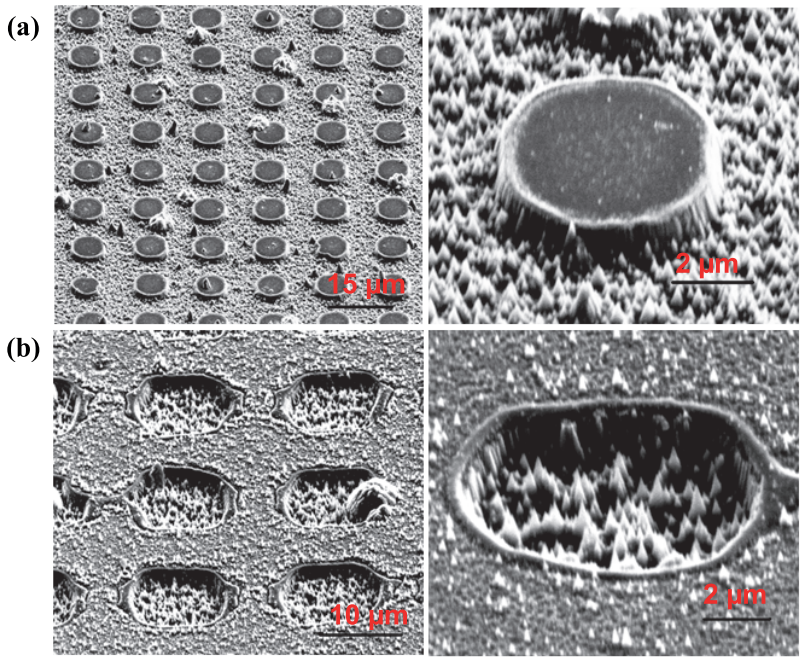

Figure 5. Conical structures formed on patterned silicon wafers. (a) nanocones on the lower regions with the protruding platform not etched, (b) cones in the concave hole with the higher regions not etched.

s is a crystal constant giving the number of atoms ejected per unit energy deposited in the surface layer of effective depth R, n is the density of atoms per unit volume, and E_a is the value of ion energy that allows the ions and atoms to approach to a distance $a = a_0/(Z_1 Z_2)^{1/6}$ in a head-on collision. a_0 is the Bohr radius of 0.053 nm; Z_1, Z_2 are the atomic numbers of the ion and the substrate, respectively.

As seen from equation (1), $S(\theta)$ raises with the increasing of incidence angle θ, when θ is smaller than a critical angle $\theta_{\max}$; yet when θ is larger than a critical angle $\theta_{\max}$, $S(\theta)$ decreases rapidly [30]. So $\theta_{\max}$ is the angle at which maximum sputtering yield should be reached. The critical angle is given by [30].

$$\theta_{\max} = \pi/2 - \frac{5a_0^2 n^{2/3} Z_1 Z_2 E_r}{(Z_1^{2/3} + Z_2^{2/3}) E_i} \tag{2}$$

a_0 is the Bohr radius, n is the substrate atom density, for diamond it is 1.757×10^{23} cm^{-3}, [20] E_i is the incident ion energy, E_r is the Rydberg constant with value of 13.6 eV, and θ is defined as the angle between the substrate normal and ion beam incidence. Therefore, a cone develops with its axial parallel to the direction of the incidence ion beam having a shank angle of

$$\alpha = \pi - 2\theta_{\max} = \frac{5a_0^2 n^{2/3} Z_1 Z_2 E_r}{\left(Z_1^{2/3} + Z_2^{2/3}\right) E_i} \tag{3}$$

Both ion density n and ion incident energy E_i are dependent on gas pressure [20]. This is the physical nature for cone angle dependence on gas pressure, which is jointly related both with plasma and material parameters.

During the plasma etching, CH_3^+ ions play a key role in general cones formation, which can be explained as follows. At high pressure (~10 Torr), ion-neutral charge exchange collision significantly affects the energy distribution of ions [31]. An ideal ion-neutral collision model was proposed and the basic assumptions of this model are shown as the following:

(1) All ions are generated from the bulk plasma, and there is no further ionization in the sheath near the substrate surface.
(2) An ion undergoing a collision loses all its kinetic energy. In each ion–neutral collision there is only charge exchange. That is, during collision the neutral at rest becomes an ion with zero velocity, and the ion becomes a neutral but retains its velocity that it has gained from the potential just prior to the collision. The energetic neutral travels towards the cathode without undergoing any further collision, as the neutral–neutral collision cross section is rather low. The newborn ion again gets accelerated towards the cathode and further undergoes charge exchange collision with neutrals. In general, an energetic ion and a stationary neutral change into a stationary ion and energetic neutral, which looks like the energetic ion changes into a stationary ion during the collision.
(3) Field distribution in the sheath is assumed as [32].

$$V(x) = -V_0 \left[(s - x)^m / s^m\right] \tag{4}$$

x is the distance from a cathode to a certain position in the sheath, $V(x)$ is the voltage at this position, s is the thickness of the plasma sheath, and m is a non-dimensional constant chosen to be 5/3. The nearer to the cathode, the higher the electric field and the ions will be accelerated to higher energy in each mean free path during their impinging onto the cathode. The highest

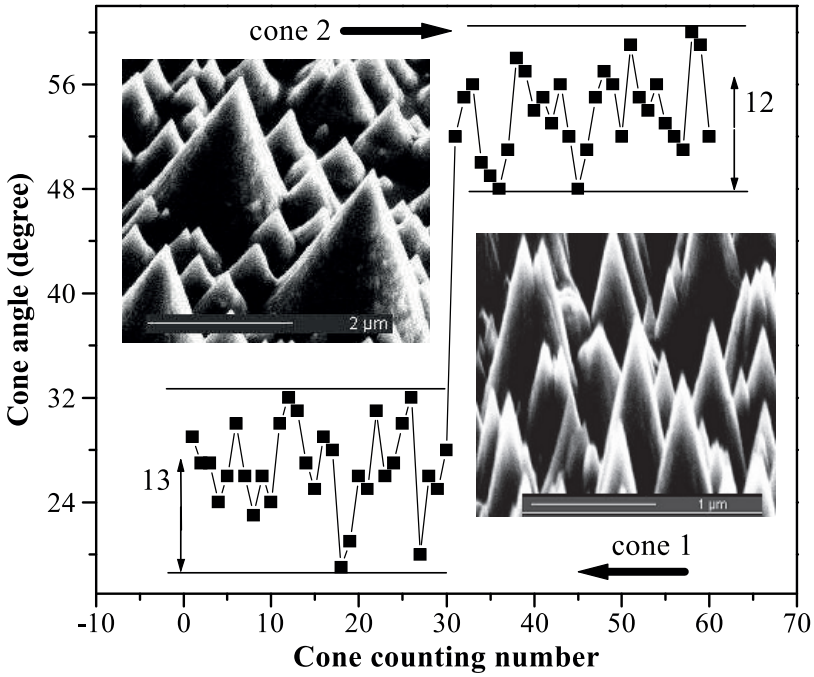

Figure 6. Silicon cones with different cone angle formed at different gas pressure. Upper inset image: the averaged cone angle is about 27° (with statistical error of about 6.5°) at gas pressure of 5 Torr. Lower inset image: the averaged cone angle is about 52° (with statistical error of about 6°) at gas pressure of 30 Torr.

field is about 0.5 V μm^{-1}, when the voltage is chosen to be 300 V and s is chosen to be 1000 μm. According to this model, all ions bombarding the cathode gain their energy in the last mean free path, and thus the energy of the ions bombarding the substrate can be obtained as follows:

$$E(w) = \int_{w}^{0} -Z\,\mathrm{d}V(x) = ZeV_0\left[1-\left(\frac{s-w}{s}\right)^{m}\right](w<\lambda)\ (\mathrm{eV}). \quad (5)$$

Z is the charge number of ions, λ is the mean free path of ions in the plasma. $E_{\max}$, the maximum energy of ions acquired in the plasma, is equal to $E(\lambda)$. It can be seen that $E_{\max}$ is increased with an increasing of λ and applied voltage. At the experimental pressure of 20 Torr, discharge current of 100 mA and bias of −300 V, the sheath thickness is calculated to be about 1000 μm. In this case, the maximum energy of CH_3^+ ions is about 210 eV, while that for H^+ ions is about 60 eV [28]. If we further note the threshold energies of H^+ and CH_3^+, ion sputterings are 15.03 and 7.37 eV, respectively [20], the proportion of H^+ energetic ions applicable for C atom sputtering is rather low, while that of CH_3^+ is much higher. In a word, for etching of diamond substrate, the sputtering rate of CH_3^+ ions is much higher than H^+ ions.

In addition, original nanostructures on the substrate also have an important effect on the cone formation during the selective plasma etching process. The CH_3^+ ion has been identified as the main building block in the flowing discussion due to the fact that the CH_3^+ ion is the dominant ion species in the methane discharges [33]. The CH_3^+ ion is generated as a result of the radical ionization of a CH_3 radical and the dissociative ionization of methane [34–36]. It should be mentioned that the other ionic building units, as long as their charge and mass would not be very much different from the methyl CH_3^+ ion, will not change the obtained distributions drastically. The movement of CH_3^+ ions is driven by the combinative electric fields produced by both the sheath and the preliminary surface nanostructures. As shown in a previous publication [37], the ion transport simulation provides important characteristics of the displacement and velocity of the ions. It is shown that a rigorous account of the realistic nanostructure shape leads to very different distribution of the ion fluxes on the nanostructured surfaces. The local ion flux distribution, which is determined by the total electric field $\vec{E}(r)$ acting on each ion impinging the surface, is a critical factor in the etching process on the substrate, and determines the nanostructure growth patterns. $\vec{E}(r)$ is expressed as [37].

$$\vec{E}(r) = \vec{E}_{\mathrm{sheath}} + \sum_{j=1}^{N}\int_{A_j}\frac{\sigma_j d_a}{4\pi\varepsilon_0 r^3}\vec{r} \quad (6)$$

σ_j and A_j are the local surface charge density and the surface area of the nanostructures, respectively. $\vec{E}_{\mathrm{sheath}}$ is the electric field of the sheath which is calculated as [37].

$$\vec{E}_{\mathrm{sheath}} = \frac{4}{3}\frac{V_{\mathrm{bias}}}{S}\left(\frac{z}{S}\right)^{1/3}. \quad (7)$$

Here, S is the sheath thickness, and z is the distance from the sheath edge. $\frac{4}{3}\frac{V_{\mathrm{bias}}}{S}$ is the maximum value of sheath field. As we see, $\vec{E}_{\mathrm{sheath}}$ is a uniformly distributed field, which can not introduce selective etching. Therefore, the second term in

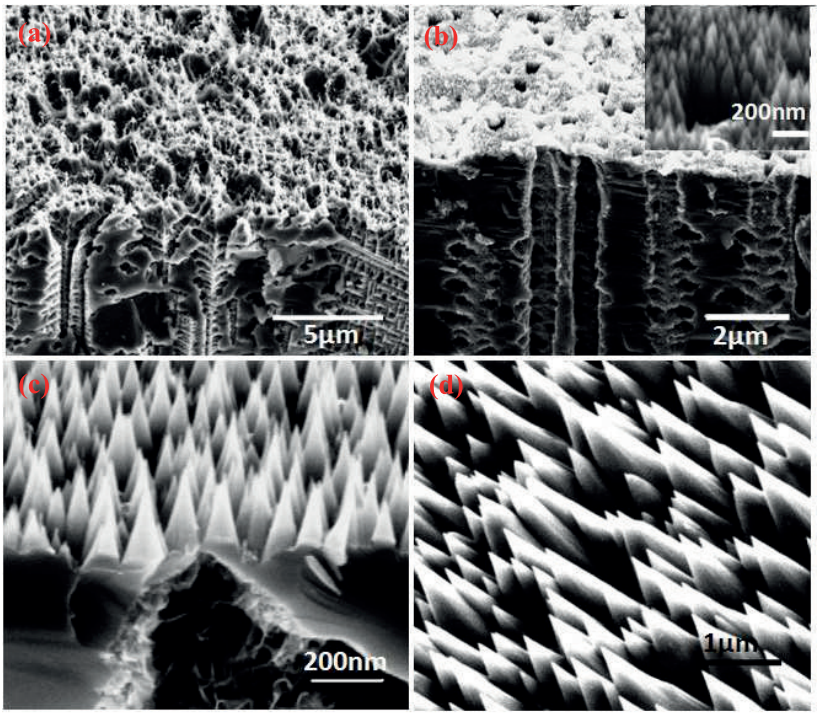

Figure 7. Cones formed on different porous silicon samples formed at etching current densities of 60 (a), 30 (b), 10 (c), and 0 mA cm^{-2} (d), respectively.

equation (6), which is determined by the preliminary surface nanostructures, must play a key role for cones formation.

The key role played by pre-manufactured surface nanostructures has been verified by the different cones morphologies formed on surfaces of silicon and porous silicon, as shown in figure 7. Porous silicon was formed using N-type silicon in a conventional Teflon cell anodization system containing HF (49%) and C_2H_5OH (95%) with a volume ratio of 1:2. The etching time is 20 min. The etching current density for the formation of different porous silicon samples is set at 60, 30, 10 and 0 mA cm^{-2}, respectively, corresponding to figure 7(a)–(d). After etching, the samples were rinsed in C_2H_5OH for a few minutes, and then they were dried in air.

The number fraction of the ions colliding with the original nanostructures and the substrate is quite different for cone arrays with different aspect ratios. It thus indicates that as-formed cones should show a cone angle with certain predominated values, which should be different for different materials. Whereas, the particles collide more frequently with the base sections compared to the top sections for all the aspect ratio arrays, which is a general result. This result coincides well with the previously formulized results that the incident energetic ions should collide more frequently with the concave sections than the convex sections [20]. It should be noted that the ions' movement is complicated and unpredictable due to the existence of the additional three-dimensional (3D) electric fields of random surface nanostructures, which indicates only a statistical method can be employed to provide a definite evidence to as-obtained experimental results. As should be re-noted here, nanoparticles masking of SiC, metal and oxides are needed to interpret the formation of conical structures in a one-step plasma etching process [19], but it is not suitable for the explanation of some others' cone-formation process, because no masking heterogeneous nanoparticles are observed in HRTEM characterizations [20, 25]. Therefore, an alternative mechanism must be established to account for the present results.

Now, we are ready to set up the selective ions etching mechanism for cone formation. The different sputtering rates for different regions of the hillock are schematically shown in figure 8. If the relation of $\overline{E} > E_{th}$ ($\overline{E}$: average ion energy; and E_{th}: sputtering threshold energy) is satisfied, sputtering of the substrate will occur. Just as shown in figure 8(a), target atoms were not usually sputtered from the exact hitting spots of the incident ions, and target atoms near the hitting spots will be sputtered out 'down-stream' due to cascade-collision for low-energy sputtering [33]. The sputtering rate of the cone tip is less than that of the cone bottom ($\nu_{top}/\nu_{bottom} < 1$), and for cones with smaller cone angle this effect becomes more apparent. As a result, different sputtering rates for different regions of the hillock can be introduced, just as shown in figure 8(b).

The occurrence of instantaneous masking during etching should be the fact of existence, no matter whether the original substrate surface is smooth or rough, although the evidence of the masking particles located on the top of the conical structure is not found in the TEM images in these one-step selective plasma etching methods. But the amorphous carbon layer with several nanometers of thickness can be found on the surface of all as-fabricated conical structures due to carbon-based CH_3^+ ion plasma etching, and a large number of random carbon particles can be formed as a temporary mask

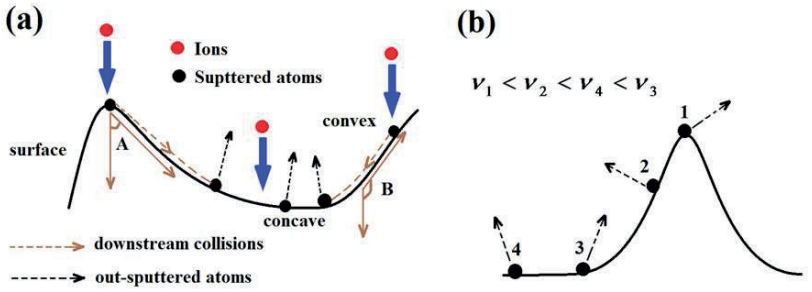

Figure 8. Illustration of cascade-collision to induce different sputtering rate of convex and concave regions. (a) Down-stream cascade-collision, (b) different sputtering rates of different regions.

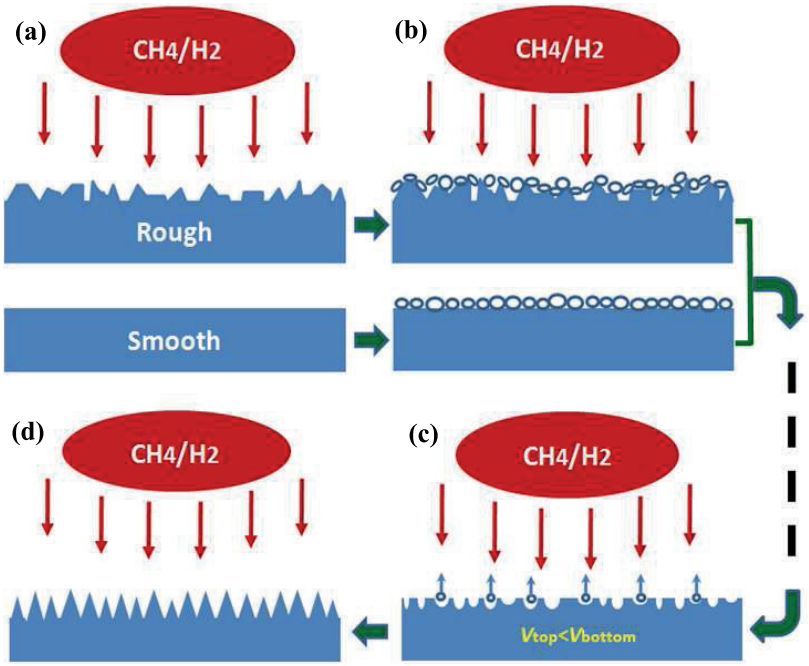

Figure 9. Illustration of instantaneous masking and selective processes. (a) pre-roughening of smooth surface, (b) instantaneous nano-carbon deposition as nanomask, (c) convex and concave development, and (d) cones formation due to selective ions etching.

and momentarily are removed by H^+ ions etching, being a competition process. This cone growth process is illustrated in figure 9. In the initial sputtering stage (figures 9(a) and (b)), the smooth surface with random masking or surface non-uniformity such as defects, roughness, etc, will be sputtered into roughened surface nanostructures [38–40]. Then cones will be formed due to an enhanced sputtering effect on the hillock bases, and cones with a larger height and a smaller cone angle will be developed by further sputtering (figures 9(c) and (d)). At last, certain dynamic equilibrium among the etching of different parts will be reached, and cones with constant height and cone angle will be developed. During the development of surface cones, a much more energetic CH_3^+ ion is identified to play a key role, while H^+ ions with lower energy are also helpful for developing the initial surface roughness. As can be seen from the above discussion, both insulating and conducting surfaces can be etched into a conical structure. As pointed out by Ostrikov [3, 41], the gas plasma is highly conductive and is favorable for efficient cluster charge dissipation upon contact with either insulating or conducting surfaces. Moreover, the substrates are usually charged negatively at the initial stage of deposition and remain negatively charged if the charge dissipation in conducting substrates is efficient. This favors the incoming of energetic positively charged nanoclusters and nucleates, and therefore the plasma provides 'equal opportunities' for impinging on insulating and conducting substrates [42]. As we see, a more thorough theoretical simulation of selective etching induced by surface nanostructures is still an active and energetic research topic.

4. Conclusion

In summary, surface conical structures can be formed on both insulating and conducting substrates in DC biased HFCVD system. The geometry-dependent etching process by CH_3^+ ion in CH_4/H_2 plasma is recognized to support the maskless selective etching model for cones formation. During the developing of surface cones, a much more energetic CH_3^+

ion is identified to play key role, while H^+ ions with lower energy are also helpful for developing the initial surface roughness. Another important role of the large amount of H^+ ions is to etch out the undesired carbon deposition; elsewhere it will introduce carbon deposition rather than the subtractive sputtering process. Instantaneously deposited nanocarbons are also needed to set up the initial surface roughness (or hillocks). The formation of microscopic cones during physical ion etching is basically due to a local non-uniformity (introduced by local surface nanostructures) of the electric field and ion etching rate. Different sputtering rates of surface convexes and concaves will develop the ever-increased conical structure, which is named as a selective sputtering mechanism. A competition will also be involved in this process: the larger cones are optimized to have a large height and small cone angle, and the lower cones will diminish last. This scheme for the formation of a surface conical structure can be generally applied to versatile materials with promising applications in many fields like a field electrons emitter, point electron injection probe, anti-reflection coating, bio-chemical sensing, as well as an optical enhancement structure for Raman spectroscopy and photo-electricity conversion.

Acknowledgments

This work was financially supported by the National Natural Science Foundation of China (NSFC) (Grant No. 11274082, 91023041, 11174362, 91323304, 51272278, 61390503), and the Shandong Excellent Young Scientist Research Award Fund Project (Grant No. BS2011CL002). Special thanks are given for the Fundamental Research Funds for the Central Universities (Grant No. HIT. BRET. 2010014) and the Knowledge Innovation Project of CAS (Grant No. KJCX2EWW02).

References

[1] Hellemans A 1996 *Science* **273** 1173
[2] Hsieh H Y, Huang S H and Liao K F 2007 *Nanotechnology* **18** 505305
[3] Ostrikov K 2005 *Rev. Mod. Phys.* **77** 489
[4] Hofmann M, Hsieh Y P and Liang C T 2013 *J. Raman Spectrosc.* **44** 81
[5] Okano K, Koizumi S, Silva S R P and Amaratunga G A J 1996 *Nature* **381** 140
[6] Li Y F, Zhang J H and Bai Y 2010 *Nano Today* **5** 117
[7] Yang Q, Hamilton T and Xiao C 2006 *Thin Solid Films* **494** 110
[8] Zou Y S, Chong Y M and Ji A L 2009 *Nanotechnology* **20** 155305
[9] Liu Y L, Jiang L and Dong H L 2011 *Small* **7** 1412
[10] Zhao Q, Xu J and Xu X Y 2004 *Appl. Phys. Lett.* **85** 5331
[11] Ji X H, Zhang Q Y and Lau S P 2009 *Appl. Phys. Lett.* **94** 173106
[12] Liu N, Wu Q and He C Y 2009 *ACS Appl. Mater. Interfaces* **1** 1927
[13] Yang S L, Gao R S and Niu P L 2009 *Appl. Phys.* A **96** 769
[14] Chang H J, Hsieh Y P and Chen T T 2007 *Opt. Express* **15** 9357
[15] Spindt C A, Brodie I, Humphrey L and Westerberg E R 1976 *J. Appl. Phys.* **47** 5248
[16] Tatarenko N I, Solntsev V A and Rodionov A N 1999 *J. Vac. Sci. Technol.* B **17** 647
[17] Poborchii V V, Tada T and Kanayama T 1999 *Appl. Phys. Lett.* **75** 3276
[18] Seeger K and Palmer R E 1999 *Appl. Phys. Lett.* **74** 1627
[19] Hsu C H, Lo H C, Chen C F, Wu C T, Hwang J S, Das D, TsaiJ, Chen L C and Chen K H 2004 *Nana Lett.* **4** 471
[20] Wang Q, Gu C Z, Li J J, Wang Z L, Shi C Y, Xu P, Zhu K and Liu Y L 2005 *J. Appl. Phys.* **97** 093501
[21] Chen Q W, Zhu D L, Wang J and Zhang Y G 2003 *Appl. Phys. Lett.* **82** 1018
[22] Fillip V, Nicolaescu D, tanemura M and Okuyama F 2001 *Ultramicroscopy* **89** 39
[23] Shieh J R, Srikanth K and Fu H 2011 *J. Phys. D: Appl. Phys.* **44** 174010
[24] Baik E-S, Baik Y-J and Jeon D 1999 *Diamond Relat. Mater.* **8** 2169
[25] Zhang W J, Meng X M, Chan C Y, Wu Y, Bello I and Lee S T 2003 *Appl. Phys. Lett.* **82** 2622
[26] Sigmund P 1973 *J. Mater. Sci.* **8** 1545
[27] Larson D J, Teng C-M, Camus P P and Kelly T F 1995 *Appl. Surf. Sci.* **87/88** 446
[28] Wang Q, Li J J, Li Y L, Wang Z L, Gu C Z and Cui Z 2007 *J. Phys. Chem.* **111** 7058
[29] Wehner G K 1965 *Adv. Electron. Electron. Phys.* **7** 239
[30] Steward A D G and Thompson M W 1969 *J. Mater. Sci.* **4** 56
[31] Phelps A V 1991 *J. Phys. Chem. Ref. Data* **20** 557
[32] SedlaOek M 1996 *Electron Physics of Vacuum and Gaseous Devices* (New York: Wiley) p 398
[33] Zhou J, Martin I T, Ayers R, Adams E, Liu D and Fisher E R 2006 *Plasma Source Sci. Technol.* **15** 714
[34] Toyoda H, Kojima H and Sugai H 1989 *Appl. Phys. Lett.* **54** 1507
[35] Levchenko I, Ostrikov K, Keidar M and Xu S 2005 *J. Appl. Phys.* **98** 064304
[36] Ostrikov K, Long J D, Rutkevych P P and Xu S 2006 *Vacuum* **80** 1126
[37] Ostrikov K 2013 *Phys. Plasmas* **20** 033501
[38] Yamamura Y and Bohdansky J 1985 *Vacuum* **35** 561
[39] Feix M, Hartmann A K and Kree R 2005 *Phys. Rev.* B **71** 125407
[40] Almen O and Bruce G 1961 *Nucl. Instrum. Methods* **11** 257
[41] Ostrikov K 2011 *J. Phys. D: Appl. Phys.* **44** 174003
[42] Gogolides E, Constantoudis V and Kokkoris G 2011 *J. Phys. D: Appl. Phys.* **44** 174021